Automatic Co-Registration of Optical Satellite Images and Airborne Lidar Data Using Relative and Absolute Orientations

Tee-Ann Teo and Shih-Han Huang

***Abstract*—Co-registration of 2-D images and 3-D lidar points in a common area is an important task in data fusion as well as other applications. As the information acquired by image and lidar systems are not the same, the registration of heterogeneous sensors is a challenging issue. The objective of this study is to perform the co-registration of 2-D images and 3-D lidar points using relative and absolute orientations. The proposed method performs image matching between stereo images for relative orientation modeling and generates a matched 3-D surface model. Then, an automatic least squares 3-D surface matching is applied between matched 3-D surface model and lidar 3-D points. Finally, the precise object-to-image transformation and orthoimages can be generated via relative and absolute transformation. The test data include WorldView-2 image, QuickBird image and lidar data. The experimental results indicate that the relative orientation may reach subpixel accuracy while the absolute orientation may reach 1 pixel accuracy. Moreover, the geometric consistency between orthoimages is better than 0.5 m on the ground.**

***Index Terms*—High resolution satellite images, least squares 3-D surface matching, lidar point clouds, registration.**

I. Introduction

ACTIVE and passive sensors are two commonly used sensors. Active sensors provide their own energy source for illumination; for example, the lidar system uses a laser scanner to acquire three-dimensional (3-D) point clouds of land surface. In comparison, passive sensors are used to detect energy that is naturally available; for example, optical sensors acquire two-dimensional (2-D) images of land surface. Therefore, the information acquired by passive optical and active lidar sensors is not the same. In many applications, different sensors must be deployed in the same area for interpretation and analysis to gain more useful knowledge for the application. Hence, co-registration is an important preprocessing [1] step in data fusion.

The development of high resolution satellites not only focuses on improving spatial and spectral resolution, but also time resolution. As most high resolution satellites are capable of body rotation to acquire in-track multi-look images, their agility enhances the capability to acquire multiple images over a given location in a single path. Moreover, the satellite constellation also offers acquisition and revisiting capacity using a number of satellites. The improved time resolution of recent satellites such as QuickBird and WorldView series can be used in object reconstruction [2], change detection [3], object tracking [4], and other applications.

Lidar is a well-established technique for deriving 3-D information for mapping and GIS tasks. The lidar system integrates a laser scanner, a Global Position System (GPS) and an Inertial Navigation System (INS), and thus is an effective technology to obtain 3-D surface models. In addition, it has a high precision laser ranging and scanning orientation made for decimeter ground surface accuracy. The accuracy of lidar data is generally sufficient to be used as reference data for geometric correction of satellite images.

In order to compensate for orientation errors of satellite images, lidar data can be applied to improve the positioning accuracy of satellite images. Moreover, the digital surface model (DSM) from lidar can be used to correct the relief displacements in ortho-rectification of satellite images. Hence, the benefits of integrated satellite images and lidar are the accuracy and automation improvement in geo-processing.

The co-registration of satellite images includes radiometric and geometric process. The radiometrical co-registration is used to obtain uniform radiometric response between images [5]. Geometrical co-registration is necessary to correct for relief displacement of terrain and distortion arising from the viewing geometry. Geometrical co-registration of lidar and images aims to provide accurate transformation between 2-D image space and 3-D lidar object space, but the process can be challenging for several reasons. The lidar system acquires shape information, while an image sensor acquires spectral information. Moreover, the acquired lidar data is in the form of 3-D points using object coordinates, while the acquired image is in the form of 2-D grid using image coordinates. Both lidar and image capture the information of land surface, but display with different representations. The lidar data uses an orthographic projection while the image data uses a perspective projection.

The direct approach to achieving co-registration of the lidar data and the imagery data would be to identify well-defined feature points which can be located in both the lidar 3-D object model, and in the 2-D imagery. The coordinates of an object point in both lidar and image data are called registration point. Registration points are used to calculate the transformation coefficients in co-registration. However, it is not easy to measure well-defined feature points from irregular lidar point clouds. In order to overcome the problem of registration points, Habib *et al.* [6] proposed to use linear features as registration

Manuscript received August 10, 2012; revised November 16, 2012; accepted December 17, 2012. Date of publication January 18, 2013; date of current version September 20, 2013. This work was supported in part by National Science Council of Taiwan. *(Corresponding author: T.-A. Teo.)*

The authors are with the Department of Civil Engineering, National Chiao Tung University, Taiwan (e-mail: tateo@mail.nctu.edu.tw).

Color versions of one or more of the figures in this paper are available online at http://ieeexplore.ieee.org.

Digital Object Identifier 10.1109/JSTARS.2012.2237543

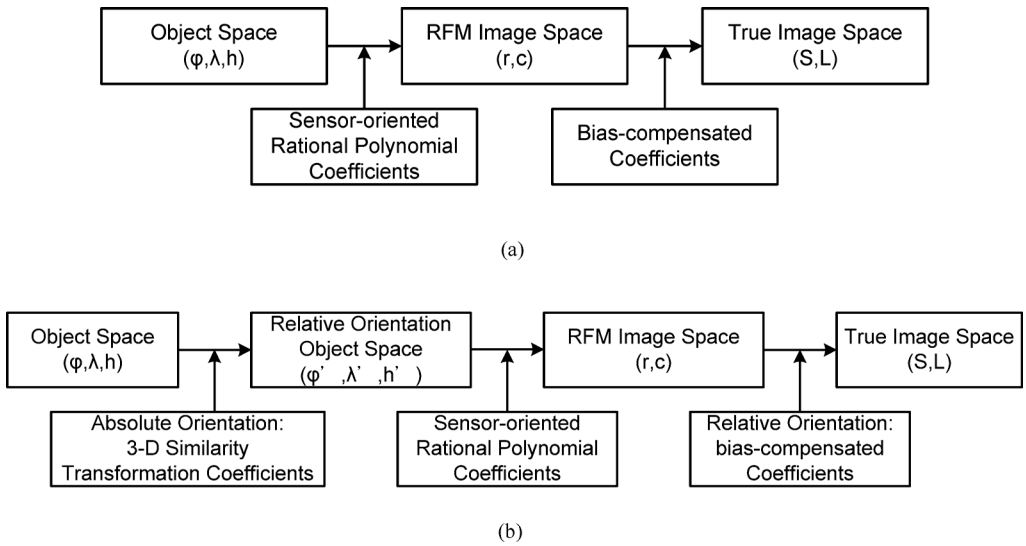

Fig. 1. Comparison of the traditional and proposed object-to-image transformation. (a) Traditional object-to-image space transformation (b) Proposed object-to-image space transformation.

entities for the registration of lidar and aerial images. Several researchers have reported on the registration of lidar and a single image. Abedini *et al.* [7] and *Toth et al.* [8] used the scale-invariant feature transform (SIFT) approach for the registration of lidar intensity data and optical imagery. Palenichka *et al.* [9] used salient image disks (SID) to extract the control points for the registration of lidar range data and a QuickBird image. Kwak *et al.* [10] performed the registration of aerial imagery and lidar data using centroids of plane roof surfaces. Lee *et al.* [11] minimized the summation of absolute difference between the edges from lidar and satellite images. Most of the studies focused on direct matching between lidar and single image via feature-based matching; relatively few studies discussed the registration of lidar and satellite stereo images.

The traditional stereoscopic mapping procedures for aerial stereo images include relative and absolute orientations [12]. Relative orientation performs image matching between stereo images, and the extracted tie point is then used to establish the relative model between stereo images [13]. It is used to determine the relative rotation angles and positional displacements between two overlapped images, as well as to obtain a relative stereo model without true world coordinates. Absolute orientation uses 3-D similarity transformation to transform the relative model into an absolute model representing a true 3-D model [14]. It uses ground control points to align the relative stereo model into real world coordinate system.

In this study, we propose an automatic approach for the registration of lidar and satellite stereo images, inspired by traditional aerial image processing. The objective is to develop an automatic co-registration procedure for lidar and satellite stereo images using relative and absolute orientations. In order to overcome the problem of different information captured from different sensors, the proposed method performs image matching between stereo images for relative orientation modeling and generates the matched 3-D surface model. Then, an automatic least squares 3-D surface matching [15] is applied between the stereo image of 3-D surface model and lidar 3-D points. Finally, the precise object-to-image transformation and orthoimages can be generated via relative and absolute transformations.

The satellite sensor model in this study is the rational function model (RFM). The coefficients of RFM are called sensor-oriented rational polynomial coefficients (RPCs), which are provided by a satellite vendor and recorded in the metadata of satellite images. Due to the standardization and simplicity, RFM has been widely used for high resolution satellite image [16]. A comparison of the traditional and proposed object-to-image space transformation (Fig. 1) shows that the traditional approach extracts the registration points between lidar and image directly and calculates the bias-compensated coefficients from registration points. In Fig. 1(a), "object space" is the ground coordinates of a point while the "true image space" indicates the real image coordinate without RFM's model errors. The 3-D ground coordinates can be transformed to RFM image coordinates using sensor-oriented RPCs in the metadata. As the sensor-oriented RPCs contain errors, we need additional bias-compensated coefficients to transform a point in RFM image space to true image space. In this approach, the sensor-oriented RPCs are recorded in the metadata while the bias-compensated coefficients are calculated from registration points between lidar and image.

Fig. 1(b) shows the idea of the proposed method. The proposed method is a two-step transformation (i.e., relative and absolute orientations) in which an object point in object space is transformed to the relative model; the point in the relative model is then further transformed to image space. In this approach, the coefficients of absolute orientation are calculated from the lidar surface and stereo image surface. The bias-compensated coefficients are calculated from registration points between satellite images. The proposed method comprises three major steps: (1) relative orientation between satellite stereo images; (2) DSM generation from satellite stereo images; and (3) absolute orientation using lidar points and image matched DSM.

Today the geolocation accuracy of high resolution satellites refers to the accuracy of the on-board global positioning system (GPS) and inertial navigation system (INS) to support direct

platform orientation. For example, QuickBird and WorldView-2 are capable of 23 m [17] and 3.5 m [18] geolocation accuracy without using ground control points (GCPs). For medium resolution satellites such as SPOT-1 to SPOT-4, the geolocation accuracies without GCPs are about 350 m [19]. The geolocation accuracy of high resolution satellite is relatively better than medium resolution satellite image. Several studies indicate that the sensor-oriented rational polynomials coefficients of satellite images have high relative accuracy [20] and, consequently, the image matched 3-D surface model closely resembles the object surface model. Moreover, the initial alignment between stereo images for relative orientation is sufficient that a manual initial tie point is not needed in these types of high resolution satellite images [21]. The initial disorientation between QuickBird and WorldView-2 images refers to the geolocation accuracy. The automatic coarse-to-fine image matching based on image pyramid is able to handle the disorientation [21].

The main motivation of this research is to verify the possibility of the co-registration of RFM-based satellite stereo images and lidar point clouds using relative and absolute orientations. The major contribution of this research is to propose an automatic procedure for the registration of lidar and satellite stereo images via relative and absolute orientations. The proposed method does not perform matching between image and lidar directly. It generates the matched 3-D surface from satellite stereo images and then applies a 3-D surface matcher to the image matched 3-D surface and lidar 3-D points for absolute orientation. This process is used to avoid the problem of different information between images and lidar.

The scope of this research is the automatism of data co-registration between stereo images and lidar point clouds. This study assumes that the stereo images contain sufficient image features for image matching and 3-D surface generation. Moreover, the 3-D surface model contains sufficient variation in height direction. The surface matching needs different elevations to determine the absolute orientation. In other words, the proposed method is not suitable for flat terrain with very little variation in elevation.

II. The Proposed Scheme

The proposed method comprises three major steps: (1) relative orientation; (2) DSM generation; and (3) absolute orientation. The workflow of proposed method is shown as Fig. 2 and the details of each step are given below.

A. Relative Orientation

Relative orientation improves the relative consistency between stereo images and also generates geometric constrained stereo model for absolute orientation. Relative orientation includes two major parts. First, area-based image matching is used to generate tie points between stereo images; second, relative orientation is carried out using the rational function model and bias compensation function [20], [22].

An area-based image matching, which calculates the similarity of gray values, is selected for tie-point generation using satellite stereo images. The initial matching uses normalized cross correlation (NCC) [23] while the precise matching uses least squares image matching [24]. In order to reduce the pull-in-

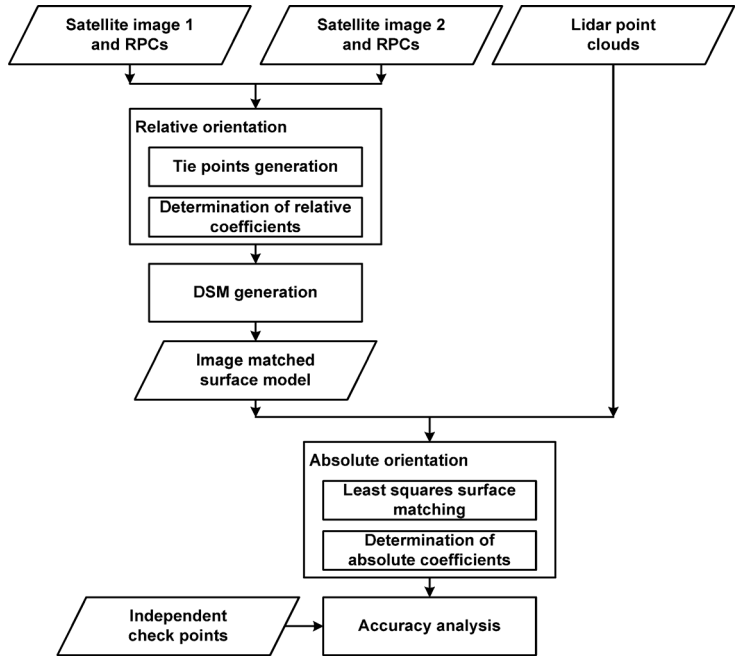

Fig. 2. Work flow of proposed method.

range at the stage of image matching, we employ an image pyramid to refine the matching results iteratively.

The RFM uses the ratio of two cubic polynomials to describe the relationship between object space and image space [25]; the RFM bias compensation model is selected for this study [26]. The bias compensation can be performed in either object space [22] or image space [26]. The object space model compensates the biases in absolute positioning via ground control points. In this study, we only have tie points as the ground control points are not available. Hence, the image space model is selected in relative orientation. Relative orientation of RFM determines the bias compensation coefficients using tie points. Equation (1) is the mathematic model of RFM. The coefficients of RFM are available in the metadata. In this study, RFM is used to describe the relationship between object coordinates and RFM's image coordinates. Equation (2) is the bias compensation equation for relative orientation. The bias compensation equation is to minimize the $(\Delta r, \Delta c)$ using bias compensation coefficients. The observations are the image coordinates of matched tie points while the unknown parameters are the bias compensation coefficients $(a_{1j}, \sim a_{6j})$ and object coordinates (φ, λ, h) of tie point [22]. For a stereo pair, a tie point can establish four observation equations. When the number of tie points is greater than 12, a least squares adjustment technique is applied to solve the unknown parameters.

$$\begin{aligned} r &= \frac{p_1(\varphi,\lambda,h)}{p_2(\varphi,\lambda,h)} \\ c &= \frac{p_3(\varphi,\lambda,h)}{p_4(\varphi,\lambda,h)} \end{aligned}, \tag{1}$$

$$\begin{aligned} L_{ij} &= r_{ij} + \Delta r_{ij} \\ S_{ij} &= c_{ij} + \Delta c_{ij} \end{aligned}, \tag{2}$$

$$\begin{aligned} \Delta r_{ij} &= a_{1j} + a_{2j} r_{ij} + a_{3j} c_{ij} \\ \Delta c_{ij} &= a_{4j} + a_{5j} r_{ij} + a_{6j} c_{ij} \end{aligned}, \tag{3}$$

where

r, c	are the image coordinates in RFM image space;
φ, λ, h	are the object coordinates;
$p_1(\,) \sim p_4(\,)$	are polynomial functions in third-order polynomials;
S, L	are the image coordinates in true image space;
$\Delta r, \Delta c$	are the biases in image space;
$a_{1j}, \sim a_{6j}$	are the bias compensation coefficients;
i	is number of point; and
j	is number of image.

B. DSM Generation

The image matching in relative orientation is used to determine a small number of well distributed tie points. The role of extracted tie points is to determinate the bias compensation coefficients in relative orientation. After relative orientation, the relationship between stereo images is established. We use a hierarchical template matching strategy for automatic DSM generation using satellite stereo images. It is used to determine dense tie points for space intersection. A coarse global DSM and image pyramid are applied to reduce the pull-in-range in image matching [27]. Image matching and DSM generation are proceeded with a coarse-to-fine strategy. Least squares image matching also applied to refine the matching accuracy [24]. Blunder error detection uses geometrical constrain to remove outliers with large disparity points. An interpolation after image matching is also applied in DSM generation. The final product of DSM generation is a large number of irregular 3-D points and interpolated DSM. Notice that, the coordinates of the generated DSM are not the true object coordinates.

C. Absolute Orientation

The relative orientation of satellite images only applies tie points. No additional ground control points are involved in relative orientation. Therefore, the coordinates of image-matched DSM are still a relative model. As the very high resolution satellite images usually have good geolocation accuracy, the coordinates of the image-matched DSM are similar to the real world coordinate. On the contrary, the lidar-derived DSM in this study represents a DSM in a real world coordinates. So, we use the lidar DSM to provide ground control information and transform the image-matched DSM from relative coordinates to the real world coordinates.

Absolute orientation is used to build up a transformation between image-matched DSM and lidar-derived DSM. Three-dimensional similarity transformation function is widely used in absolute orientation. As both data represent the shape of the surface, a least squares 3-D surface matching is applied to determine the transformation parameters from relative model to absolute model.

The traditional absolute orientation measures the 3-D registration points between image-matched and lidar surfaces; the transformation coefficients are then calculated from 3-D registration points. As the aim of this research is to improve the automation of the data co-registration, we use a least squares 3-D surface matching approach to find the conjugate surfaces between image-matched and lidar surfaces.

Least squares 3-D surface matching was developed by Gruen and Akca [15]. This method assumes that two surfaces are created from the same object by different processes. In this study, one surface acquired by lidar is called the template surface $f(x, y, z)$, while the other surface from image matching is called the search surface $g(x_0, y_0, z_0)$. If the error function $e(x, y, z)$ is zero, these two surfaces should be the same, and all the patch surface in the template surface can correspond to the patch surface in the search surface as shown in (4).

In reality, the two surfaces are not totally equal. We use error function $e(x, y, z)$ to describe the inconsistency between the two conjugate surfaces. Hence, (4) can be rewritten as (5). In order to minimize the error function $e(x, y, z)$, the coordinate system of the image-matched DSM (x_0, y_0, z_0) are being subjected to a general 3-D translation, scaling and rotation transformation (the so called "similarity transformation"). It is used to minimize the integrated squared error function between these two conjugate surfaces over a well define common spatial domain. The transformation parameters of similarity transformation include a translation vector (t_x, t_y, t_z), three rotation angles (ω, ϕ, κ) and one scale factor. These parameters are used to minimize the errors between these two conjugate surfaces.

$$f(x, y, z) = g(x_0, y_0, z_0), \tag{4}$$

$$f(x, y, z) - e(x, y, z) = g(x_0, y_0, z_0), \tag{5}$$

$$\begin{aligned} x &= t_x + m(r_{11}x_0 + r_{12}y_0 + r_{13}z_0) \\ y &= t_y + m(r_{21}x_0 + r_{22}y_0 + r_{23}z_0) \\ z &= t_z + m(r_{31}x_0 + r_{32}y_0 + r_{33}z_0), \end{aligned} \tag{6}$$

where

$f(x, y, z)$ and $g(x, y, z)$	are the template and search surfaces;
$e(x, y, z)$	is error vector;
(x, y, z)	are the coordinate system of lidar-derived surface;
(x_0, y_0, z_0)	are the coordinate system of image-matched surface;
t_x, t_y, and t_z	are the three translation parameters along three axes;
$r_{11} \sim r_{33}$	are elements of the rotation matrix formed by three rotation angles ω, ϕ, and κ around three axes; and
m	is the scale factor we assume is close to 1.

The image matched 3-D points and lidar 3-D points are structuralized by a voxel structure. The points located in a voxel are used to calculate the normal vectors and plane equations for surface matching. We iteratively minimize the sum of squared errors between image-matched and lidar surface using least squares 3-D matching approach. A more in depth description of

TABLE I
INFORMATION RELATED TO TEST IMAGES

Sensor	QuickBird	WorldView-2
Level	Standard	Standard
Acquisition date	2007/11/11	2011/10/09
GSD (m)	0.6	0.50
Spectral information	Pan	Pan
Elevation angle(^{0})	62.3	67.9
Azimuth angle(^{0})	10.0	257.5
Number of check point(Absolute orientation)	50	50
Number of Check tie point(Ortho image)	50	50
Convergence angle(^{0})		49.8
Base-to-height ratio		0.93

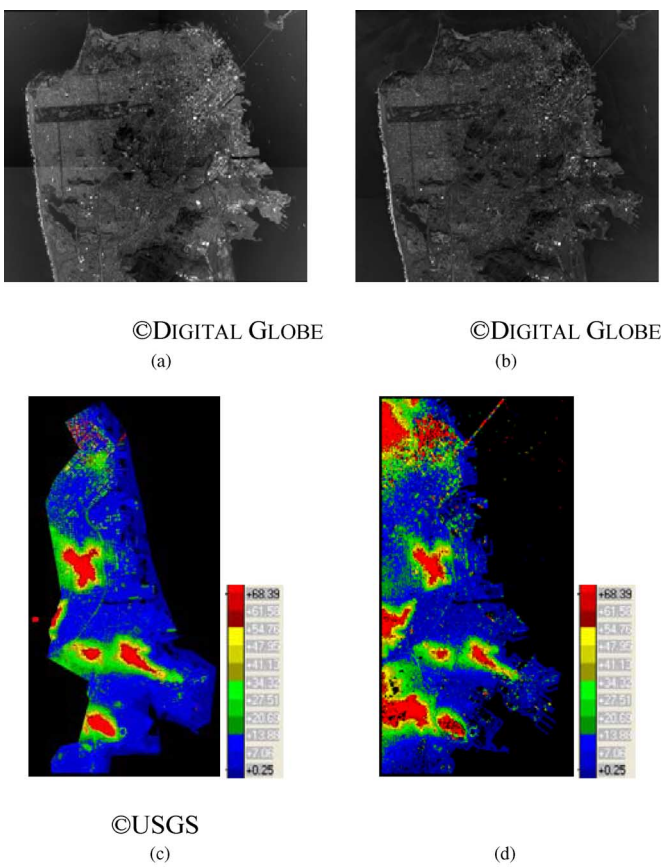

Fig. 3. Test data and matched result. (a) QuickBird Image. (b) WorldView-2 Image. (c) Lidar 3-D Points. (d) Matched 3-D Points.

the least squares adjustment details, in regards to the parameters determination can be found in Akca (2007) [28].

III. EXPERIMENTAL RESULT

The test data include very high resolution satellite images and lidar data from the IEEE 2012 Data Fusion Contest [29]. The test area is located in downtown San Francisco, California. The satellite images are WorldView-2 and QuickBird panchromatic satellite images provided by DigitalGlobe. The test images (Fig. 3(a) and (b)) show that the base-to-height ratio for this stereo pair is about 0.93. The related parameters for the rest of the images were summarized (Table I). The lidar data acquired by Optech ALTM 3100 in June 2010 (provided by USGS) show that the area of lidar data is about 30 km^2 and the average point density is about 2 pts/m^2. The elevation of the test site has about 70 m relief (Fig. 3(c)).

The validation experiments are carried out in three parts. First, the geometrical consistency after relative orientation is evaluated; second, the absolute accuracy is examined and third, orthoimages generated from the proposed methods are checked. The independent check points for absolute accuracy and check tie points for orthoimage assessment are acquired by manual measurements.

A. Accuracy of Relative Orientation

The first step of relative orientation is to extract tie points by image matching. The image pyramid has five layers. The target and search windows for NCC are 7 pixels and 21 pixels, respectively. The correlation threshold of NCC is 0.8. After NCC initial matching, least squares image matching is applied to refine the matching results. The window size for least squares image matching is 21 pixels.

As these two images are 100% overlapped, 39 well-distributed tie points are extracted and checked manually. Since these two images are georeferenced by satellite's on-board data, the initial geolocation of these two images is more accurate than 23 m without terrain effect [17], [18]. The result indicates that all of the automatic tie points are correct.

These tie points are used to calculate the bias compensation coefficients a_1–a_6 in (3). Equation (7) is used to evaluate the accuracy and suitability of this bias compensation model. The accuracy of relative orientation using an automatic matching and RFM bias compensation model (Table II) show that the root-

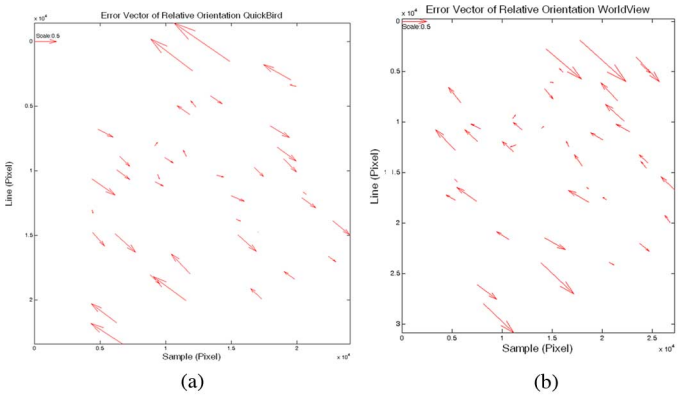

Fig. 4. Error vector of relative orientation modeling. (a) Error vector of QuickBird (b) Error vector of Worldview-2.

TABLE II
ACCURACY OF RELATIVE ORIENTATION (UNIT: PIXEL)

Number of points: 39	QuickBird		WorldView-2	
	Sample	Line	Sample	Line
Mean	0	0	0	0
RMSE	0.41	0.31	0.34	0.30
Max	1.24	0.87	0.93	0.83

mean-square errors (RMSEs) for both images achieved subpixel accuracy. These results (Table II) indicate that the bias compensation model is suitable for relative orientation. Moreover, the matching tie points for relative orientation may reach subpixel accuracy. Fig. 4 shows the error vector of relative orientation modeling.

$$\begin{aligned} V_l &= r + a_1 + a_2 r + a_3 c - L \\ V_s &= c + a_4 + a_5 r + a_6 c - S \end{aligned}, \tag{7}$$

where

V_l, V_s are the residuals of relative orientation in image space

r, c are the image coordinates in RFM image space;

S, L are the image coordinates of tie points in true image space; and

$a_1, \sim a_6$ are the bias compensation coefficients.

B. Accuracy of Absolute Orientation

After relative orientation, this study uses a commercial software ERDAS eATE [30] to generate surface models. The area for image matching is the same as lidar data, and the test area is about 10 km × 5 km. The total number of matched 3-D points is 3 801 376 and the average point density is 0.2 pts/m^2. As these two satellite images were taken in 2007 and 2011, some changed areas may affect the matching results. The matching rate in this study is about 62%, indicating that the feature is significant and correlation is high. The matching rate means the successful rate in image matching. The study area covers homogeneous ocean area. The homogeneous area usually does not have significant features for matching. As the ocean area is about 40% of study area, 62% matching rate is relatively high in this study case. We subset a small area of matched and lidar points for comparison (Fig. 5). We only have two images for image matching and, consequently, the point density is lower than lidar, especially in the homogeneous area. In addition to the point density, these two surface models look similar and can be used for surface matching.

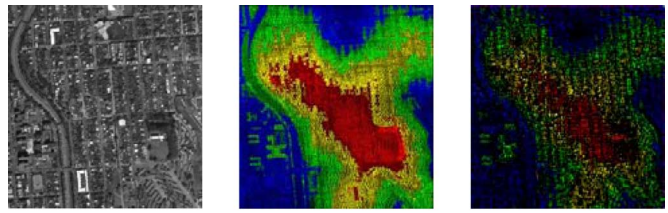

Fig. 5. Comparison of lidar and matched 3-D points. (a) Reference image. (b) Lidar points. (c) Matched points.

We employ least squares 3-D surface matching, an automatic surface registration process that iteratively minimizes the difference between image-matched and lidar surfaces, to determine the coefficients of 3-D similarity transformation. The stopping criterion of the iterative process depends on whether the unknown parameters are the same during the iteration. Although the point density of lidar and matched points of building and road profiles before and after surface matching are not the same (Fig. 6), surface matching is able to transform the matched points into lidar object space.

We carefully select 50 independent check points collected from lidar surface, lidar intensity, and satellite images to evaluate the object-to-image transformation. To avoid the problem of height discontinuous in check point selection, we mainly select the well-defined check points on the ground surface. These check points are mainly located at the area of road marks. The elevation of check points is ranged from 0 m to 70 m. The object-to-image transformation (Fig. 1(b)) integrates the coefficients of 3-D similarity transform, sensor-oriented rational polynomial coefficients provided by satellite vendor, and bias-compensation coefficients in relative orientation.

The accuracy of object-to-image transformation using the proposed method (Table III) shows that before absolute orientation the RMSEs of check points for QuickBird and WorldView-2 in sample and line direction are ranged from 1 to 9 pixels; after absolute orientation, the RMSE of check point improved to 1 pixel. The RMSE for both images achieved 1 pixel accuracy in the sample and line direction, respectively. The experimental results indicate that the 3-D similarity transformation is suitable for the transformation from relative model to absolute model. Moreover, least squares 3-D surface matching is able to build up the relationship between the two surfaces. Fig. 7 shows the error vector of absolute orientation modeling. The directions of error vectors indicate that no systematic error in the absolute orientation.

In the computation time analysis, we use a personal computer with a 3.60 GHz CPU and 16 GB Memory for relative orientation, DSM generation and absolute orientation. Relative orienta-

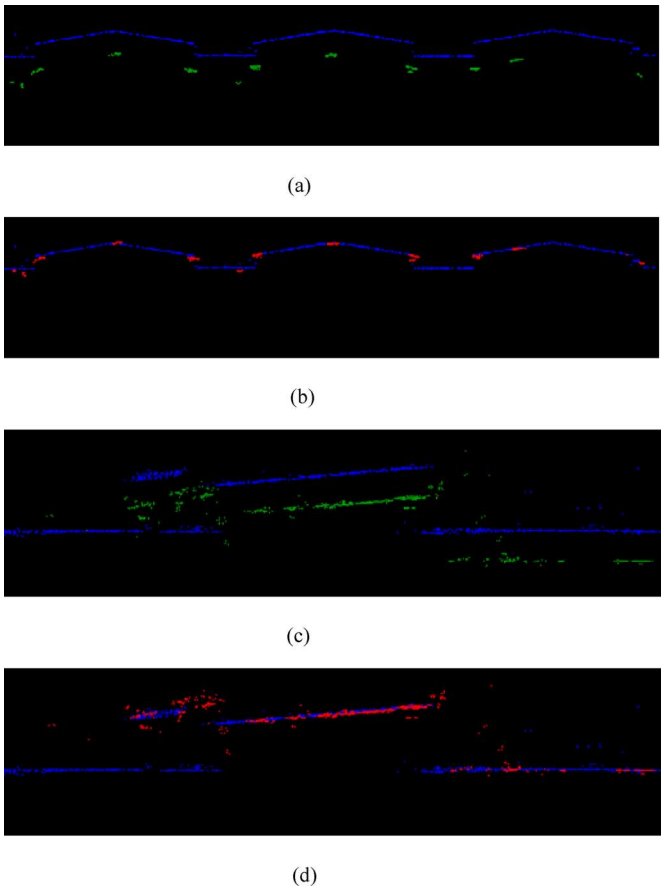

(a) (b) (c) (d)

Fig. 6. Comparison of lidar and matched 3-D points before and after surface matching. (a) Building profile before surface matching (Blue: lidar; Green: original point). (b) building profile after surface matching (Blue: lidar; Red: transformed point). (c) road profile before surface matching (Blue: lidar; Green: original point). (d) road profile after surface matching (Blue: lidar; Red: transformed point).

tion includes image matching for tie points and parameter determination for bias compensate model. The total time is about 10 minutes and most of the computation time is spent on pyramid image matching. DSM generation is time consuming, as it is a dense-points extraction process. It takes 180 minutes to extract 3.8 million points on a 10 km × 5 km area. Absolute orientation includes structuralization of irregular points, calculation of plane equation from voxel and least squares 3-D matching for similarity transformation. The computation time for absolute orientation is about 60 minutes and most of the computation time is spent on plane equation calculation. In this study, we have spent 250 minutes computation time to obtain high accurate transformation parameters between satellite images and lidar data automatically.

C. Effect of Point Density

In image matching, the difference between spatial resolution images, called scale factor, is important. This problem also occurs in 3-D surface matching, in which the difference of point density between two surfaces is also an important factor.

In order to evaluate the impact of point density, we reduce the lidar and matched points into different point densities. The image matching usually matches the top of the object; hence, the point reduction only samples the highest point in different

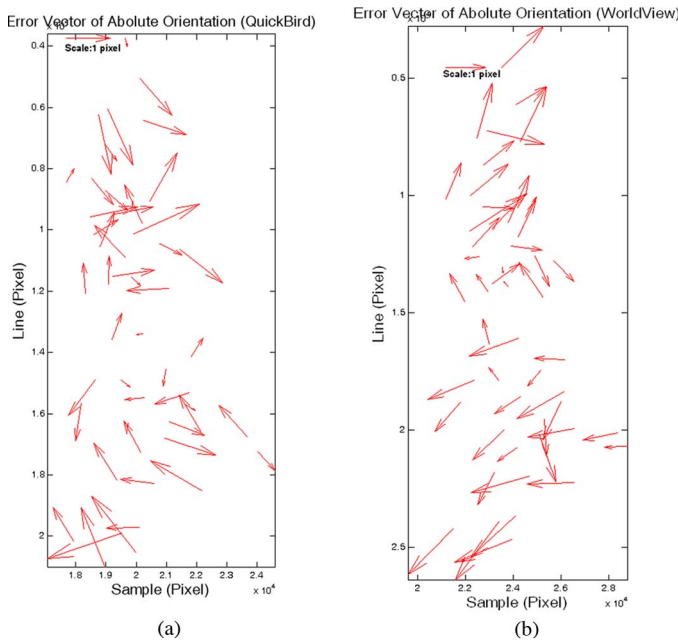

(a) (b)

Fig. 7. Error vectors of absolute orientation modeling. (a) Error vectors of QuickBird. (b) Error vectors of Worldview-2.

TABLE III
ACCURACY OF ABSOLUTE ORIENTATION (UNIT: PIXEL)

Number of check points: 50		QuickBird		WorldView-2	
		Sample	Line	Sample	Line
Before Absolute Orientation	Mean	-2.300	8.776	5.772	-0.464
	RMSE	2.698	8.829	5.802	1.019
	Max	5.394	11.868	7.793	3.360
After Absolute Orientation	Mean	0.058	-0.106	-0.168	0.004
	RMSE	0.840	0.788	1.003	0.926
	Max	2.099	1.682	2.749	1.888

grid sizes. The highest density of the image matched surface is 0.2 pts/m^2; therefore, the point densities in this analysis are 0.2, 0.1, 0.05, and 0.025 pts/m^2. We use 50 manually selected independent check points to evaluate the object-to-image transformation. A summary of different point densities (Table IV) indicates that the accuracy of check points improved as the point density increased and that the point density is a significant factor in 3-D surface matching.

D. Geometric Consistency of Orthoimages

The objective of this research is to generate accurate transformation coefficients between images and lidar. Besides, we can also use the transformation coefficients in orthorectification. In order to check the geometric consistency between 2-D images and 3-D lidar data, we use lidar DSM in satellite image orthorectification. The coefficients of object-to-image transformation are the results of relative and absolute orientations. If

TABLE IV
ACCURACY OF ABSOLUTE ORIENTATION IN DIFFERENT POINT DENSITIES (UNIT: PIXEL)

Number of check points: 50	QuickBird RMSE			WorldView-2 RMSE		
Pts/m^2	Sample	Line	2D	Sample	Line	2D
0.200	0.840	0.788	1.152	1.003	0.926	1.365
0.100	1.710	1.160	2.066	1.720	1.330	2.174
0.050	2.705	1.527	3.106	2.370	1.650	2.888
0.025	2.720	1.830	3.278	2.600	1.851	3.192

the images and lidar are well co-registrated, then, the tie point appears at the same position in orthoimages.

We generate three types of orthoimages. The first uses only the sensor-oriented rational polynomial coefficients (RPCs) to generate orthoimages; the second integrates RPCs and coefficients of relative orientation; the third combines RPCs and coefficients of relative and absolute orientations. Orthoretification is used to remove the terrain distortion and convert the perspective projection into orthographic projection. The orthorectification yields map-accurate image with real world coordinates. The research generates QuickBird and WorldView-2 orthoimages from orientation parameters (relative and absolute orientations) and lidar surface models. Then, we overlap these two orthoimages to check the geometric consistence. The discrepancy in orthoimages is small when the transformation between image and lidar is accurate. These three types of orthoimages (Fig. 8) indicate that orthoimages that use only RPCs may cause significant displacement (Fig. 8(c)). This phenomenon is especially obvious when the terrain is steep. Relative orientation improves the relative accuracy between images (Fig. 8(d)); however, there is no connection between relative orientation and lidar surface. High consistency is evident between the two orthoimages as the absolute orientation establishes the relationship between image-matched and lidar surfaces (Fig. 8(e)).

We manually select 50 check tie points in orthoimages to evaluate the geometric consistency and choose a pair of tie points that appeared in the two orthoimages. The distance between these two ground positions is used to evaluate the discrepancy (Table V). The result of RPC is about 25 m, but after relative orientation, the discrepancy is reduced to 5 m. Finally, the discrepancy is reduced to 0.5 m (about 1 pixel) when absolute orientation is applied. The experimental results indicate that the proposed method can achieve high accuracy.

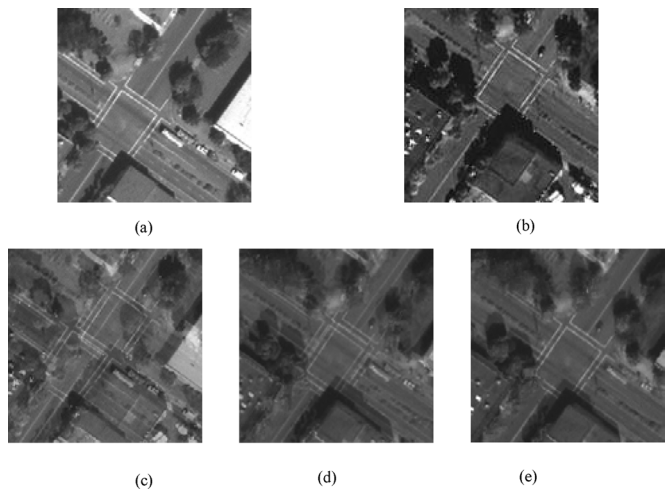

Fig. 8. Comparison of different types of orthoimages. (a) WorldView-2 image. (b) QuickBird image. (c) Overlapped orthoimages (RPCs only). (d) Overlapped orthoimages (RPCs and relative orientation). (e) Overlapped orthoimages (RPCs, relative and absolute orientations).

TABLE V
COMPARISON OF GEOMETRICAL CONSISTENCY BETWEEN QUICKBIRD AND WORLDVIEW-2 IMAGES (UNIT: METER)

	RPC only			Only the relative orientation correction			Relative and absolute orientations correction		
	dE	dN	2D	dE	dN	2D	dE	dN	2D
Mean	14.03	12.23	23.13	4.80	0.45	4.84	0.01	0.35	0.51
RMSE	16.84	17.12	24.01	4.85	0.56	4.88	0.34	0.41	0.53
Max	21.10	32.37	10.46	6.17	1.05	6.17	0.67	0.70	0.87

IV. CONCLUSION

In this study, we proposed an automatic co-registration procedure for very high resolution satellite stereo images and lidar point clouds. The proposed method consists of three major steps: (1) image matching for relative orientation, (2) image matching for DSM generation, and (3) 3-D surface matching for absolute orientation. The proposed method does not perform the matching between image and lidar data directly. The advantage is to avoid the problem of different acquired information between images and lidar; the limitation of this research is that the images in use should be multi-images. Moreover, flat terrain with very little elevation variation is not suitable for absolute orientation. In this study, the test images have high geolocation accuracy, therefore, there is no need for initial manual-measured tie points. In case the geolocation accuracy of images is not good enough, manual intervention is needed.

The experimental results indicate that relative orientation may reach subpixel accuracy while absolute orientation may reach 1 pixel accuracy. Moreover, the geometric consistency

between orthoimages may reach 0.5 m on the ground. Test results indicate that the proposed method is feasible and rigorous. This study also analyzes the impact of point density in 3-D surface matching. The quality of image-matched 3-D points may affect the registration accuracy.

This model can be applied to other satellite images and surface data. This study uses optical images to generate matched DSM for surface matching. As the radar images can also generate DSM, future work will focus on the co-registration of stereo radar images and range data.

ACKNOWLEDGMENT

The authors would like to thank DigitalGlobe and USGS for providing the imagery used in this study, and the IEEE GRSS Data Fusion Technical Committee for organizing the 2012 Data Fusion Contest.

REFERENCES

[1] B. Zitová and J. Flusser, "Image registration methods: A survey," *Image and Vision Computing*, vol. 21, no. 977–1000, 2003.
[2] G. A. Licciardi *et al.*, "Retrieval of the height of buildings from WorldView-2 multi-angular imagery using attribute filters and geometric invariant moments," *IEEE J. Sel. Topics Appl. Earth Observ. Remote Sens.*, vol. 5, no. 1, pp. 71–79, 2012.
[3] F. Bovolo, "A multilevel parcel-based approach to change detection in very high resolution multitemporal image," *IEEE Geosci. Remote Sens. Lett.*, vol. 6, no. 1, pp. 33–37, 2009.
[4] B. Salehi, Y. Zhang, and M. Zhong, "Automatic moving vehicles information extraction from single-pass WorldView-2 imagery," *IEEE J. Sel. Topics Appl. Earth Observ. Remote Sens.*, vol. 5, no. 1, pp. 135–145, 2012.
[5] Y. Li and C. H. Davis, "Pixel-based invariant feature extraction and its application to radiometric co-registration for multi-temporal high-resolution satellite imagery," *IEEE J. Sel. Topics Appl. Earth Observ. Remote Sens.*, vol. 4, no. 2, pp. 348–360, 2011.
[6] A. F. Habib *et al.*, "Photogrammetric and LIDAR data registration using linear features," *Photogramm. Eng. Remote Sens.*, vol. 71, no. 6, pp. 699–707, 2005.
[7] A. Abedini, M. Hahn, and F. Samadzadegan, "An investigation into the registration of LIDAR intensity data and aerial images using the SIFT approach," *Int. Archives Photogrammetry, Remote Sensing and Spatial Information Sciences*, vol. 37, no. B1, pp. 169–174, 2008.
[8] C. Toth, H. Ju, and D. Grejner-Brezezinsk, "Matching between different image domains," *Lecture Notes on Computer Science*, vol. 6952, pp. 37–47, 2011.
[9] R. M. Palenichka and M. B. Zaremba, "Automatic extraction of control points for the registration of optical satellite and lidar images," *IEEE Trans. Geosci. Remote Sens.*, vol. 48, no. 7, pp. 2864–2879, 2010.
[10] T.-S. Kwak *et al.*, "Registration of aerial imagery and aerial LiDAR data using centroids of plane roof surfaces as control information," *KSCE J. Civil Eng.*, vol. 10, no. 5, pp. 365–370, 2006.
[11] J. Lee, C. Lee, and K. Yu, "Autoregistration of high-resolution satellite imagery using lidar intensity data," *KSCE J. Civil Eng.*, vol. 15, no. 2, pp. 375–384, 2011.
[12] P. R. Wolf and B. A. Dewitt, *Elements of Photogrammetry with Applications in GIS*, 3rd ed. New York: McGraw-Hill, 2000.
[13] T. Liang and C. Heipke, "Automatic relative orientation of aerial images," *Photogramm. Eng. Remote Sens.*, vol. 62, no. 1, pp. 47–55, 1996.
[14] D. Rosenholm and K. Torlegard, "Three-dimensional absolute orientation of stereo models using digital elevation model," *Photogramm. Eng. Remote Sens.*, vol. 54, no. 10, pp. 1385–1389, 1988.
[15] A. Gruen and D. Akca, "Least squares 3D surface and curve matching," *ISPRS J. Photogramm. Remote Sens.*, vol. 59, no. 3, pp. 151–174, 2005.
[16] OGC, "The OpenGIS abstract specification—Topic 7: The earth imagery case, version 4," OpenGIS Consortium pp. 14–16, 1999.
[17] DigitalGlobe, QuickBird Spacecraft Datasheet. 2012 [Online]. Available: http://www.digitalglobe.com/downloads/QuickBird-DS-QB-Web.pdf
[18] DigitalGlobe, WorldView-2 Spacecraft Datasheet. 2012 [Online]. Available: http://www.digitalglobe.com/downloads/WorldView2-DS-WV2-Web.pdf
[19] CNES, "Accuracy and coverage combined of SPOT image," SPOT Image. 2005 [Online]. Available: http://www.isis-cnes.fr/pages/statique/spotProduct_en.pdf
[20] C. S. Fraser and H. B. Hanley, "Bias-compensated RPCs for sensor orientation of high-resolution satellite imagery," *Photogramm. Eng. Remote Sens.*, vol. 71, no. 8, pp. 909–915, 2005.
[21] S. R. Lee, "A coarse-to-fine approach for remote-sensing image registration based on a local method," *Int. J. Smart Sens. Intell. Syst.*, vol. 3, no. 4, pp. 690–702, 2010.
[22] H.-G. Sohn, C.-H. Park, and H. Chang, "Rational function model-based image matching for digital elevation models," *Photogramm. Rec.*, vol. 20, no. 112, pp. 366–383, 2005.
[23] T. Schenk, *Digital Photogrammetry*. Laurelville, OH: TerraScience, 1999.
[24] A. Gruen, "Adaptive least squares correlation: A powerful image matching technique," *South African J. Photogramm., Remote Sens. Cartogr.*, vol. 14, no. 3, pp. 175–187, 1985.
[25] C. V. Tao and Y. Hu, "A comprehensive study of the rational function model for photogrammetric processing," *Photogramm. Eng. Remote Sens.*, vol. 67, no. 12, pp. 1347–1357, 2001.
[26] C. S. Fraser and H. B. Hanley, "Bias compensation in rational function for IKONOS satellite imagery," *Photogramm. Eng. Remote Sens.*, vol. 69, no. 1, pp. 53–57, 2003.
[27] L. C. Chen and J. Y. Rau, "A unified solution for digital terrain model and orthoimage generations from SPOT stereopairs," *IEEE Trans. Geosci. Remote Sens.*, vol. 31, no. 6, pp. 1243–1252, 1993.
[28] D. Akca, *Least Squares 3D Surface Matching*. ETH Zurich, Switzerland: Inst. Geodesy and Photogrammetry, 2007.
[29] IEEE, "2012 IEEE GRSS data fusion contest," [Online]. Available: http://www.grss-ieee.org/community/technical-committees/data-fusion/data-fusion-contest/
[30] "User's guide of enhanced automatic terrain extraction (eATE)," Erdas Imagine p. 48, 2010.

Tee-Ann Teo received the M.S.E. and Ph.D. degrees from the Department of Civil Engineering, National Central University, Taiwan, in 2002 and 2008, respectively.

He was with the Center for Space and Remote Sensing Research, National Central University, as a Postdoctoral Research Fellow in 2008. He is currently an Assistant Professor with the Department of Civil Engineering, National Chiao Tung University, Hsinchu, Taiwan. His research activities are focused on cyber city modeling, geometrical data processing for remotely sensed data, and lidar processing.

Shih-Han Huang received the B.S. degree from the Department of Geomatics, National Cheng Kung University, Taiwan, in 2010, and the M.S.E. degree from the Department of Civil Engineering from National Chiao Tung University, Taiwan, in 2012.

His research activities are focused on lidar processing.